Title

Blocking integrin α4β7-mediated CD4 T cell recruitment to the intestine and liver protects mice from western diet-induced non-alcoholic steatohepatitis

Journal

Journal of Hepatology, 73(5)

ISSN

0168-8278

Authors

Rai, Ravi P
Liu, Yunshan
Iyer, Smita S
et al.

Publication Date

2020-11-01

DOI

10.1016/j.jhep.2020.05.047

Peer reviewed

HHS Public Access

Author manuscript

J Hepatol. Author manuscript; available in PMC 2021 November 01.

Published in final edited form as:

J Hepatol. 2020 November ; 73(5): 1013–1022. doi:10.1016/j.jhep.2020.05.047.

Blocking integrin $\alpha_4\beta_7$-mediated CD4 T cell recruitment to the intestine and liver protects mice from western diet-induced non-alcoholic steatohepatitis

Ravi P. Rai[1,*], **Yunshan Liu**[2,*], **Smita S. Iyer**[3,4,5], **Silvia Liu**[1,6], **Biki Gupta**[1], **Chirayu Desai**[7], **Pradeep Kumar**[2], **Tekla Smith**[2], **Aatur D. Singhi**[6,8], **Asma Nusrat**[9], **Charles A. Parkos**[9], **Satdarshan P. Monga**[1,6,10], **Mark J. Czaja**[2], **Frank A. Anania**[11], **Reben Raeman**[1,6]

[1]Division of Experimental Pathology, Department of Pathology, University of Pittsburgh, Pittsburgh, PA USA

[2]Division of Digestive Diseases, Department of Medicine, Emory University, Atlanta, GA USA

[3]Center for Comparative Medicine, School of Veterinary Medicine, University of California, Davis, CA USA

[4]California National Primate Research Center, University of California, Davis, CA USA

[5]Department of Pathology, Microbiology, and Immunology, University of California, Davis, CA USA

[6]Pittsburgh Liver Research Center, University of Pittsburgh, Pittsburgh, PA, USA

[7]Department of Biological Sciences, P. D. Patel Institute of Applied Sciences, Charotar University of Science and Technology, Gujarat, India

[8]Division of Anatomic Pathology, Department of Pathology, University of Pittsburgh School of Medicine, Pittsburgh, PA USA

[9]Department of Pathology, University of Michigan, Ann Arbor, MI USA

Corresponding Author: Reben Raeman, M.S., Ph.D., Assistant Professor, 200 Lothrop Street, S408 BST, Pittsburgh, PA 15261, Phone: 412-648-2021, reben.rahman@pitt.edu.

*Contributed equally

Author Contributions.

R.R. conceived the project, designed and performed experiments, analyzed data and wrote the manuscript.
F.A.A. provided valuable suggestions and scientific editing
M.J.C. provided valuable suggestions and scientific editing
S.P.M provided valuable suggestions
C.A.P. provided valuable suggestions, provided knockout mice.
A.S.N. provided valuable suggestions.
S.S.I. helped in planning and performing flow cytometric analysis
A.D.S. provided human tissue
R.P.R. maintained mouse colonies, performed experiments
Y.L. maintained mouse colonies, performed experiments, collected metabolic data
C.D. analyzed microbial data
B.K. maintained mouse colonies, performed experiments
S.L. analyzed RNAseq data
T.S. performed histochemical staining
P.K. provided valuable suggestions

Conflict of interest: All authors declare no conflicting interests.

[10]Division of Gastroenterology, Hepatology and Nutrition, Department of Medicine, University of Pittsburgh School of Medicine, Pittsburgh, PA USA

[11]Division of Gastroenterology and Inborn Error Products, Food and Drug Administration, Silver Spring, MD USA.

Abstract

Background & Aims: The heterodimeric integrin receptor $\alpha_4\beta_7$ regulates CD4 T cell recruitment to inflamed tissues, but its role in the pathogenesis of nonalcoholic steatohepatitis (NASH) is unknown. Here we examined the role of $\alpha_4\beta_7$-mediated recruitment of CD4 T cells to the intestine and liver in NASH.

Methods: Male littermate *F11r*$^{+/+}$ (control) and junctional adhesion molecule A knockout *F11r*$^{-/-}$ mice were fed a normal diet or a Western diet (WD) for eight weeks. Liver and intestinal tissues were analyzed by histology, qRT-PCR, 16s rRNA sequencing and flow cytometry. Colonic mucosa-associated microbiota was analyzed using 16s rRNA sequencing. Liver biopsies from NASH patients were analyzed by confocal imaging and qRT-PCR.

Results: WD-fed knockout mice developed NASH and had increased hepatic and intestinal $\alpha_4\beta_7^+$ CD4 T cells relative to control mice which developed mild hepatic steatosis. The increase in $\alpha_4\beta_7^+$ CD4 T cells was associated with markedly higher expression of the $\alpha_4\beta_7$ ligand mucosal addressin cell adhesion molecule 1 (MAdCAM-1) in the colonic mucosa and livers of WD-fed knockout mice. Elevated MAdCAM-1 expression correlated with increased mucosa-associated Proteobacteria in the WD-fed knockout mice. Antibiotics reduced MAdCAM-1 expression indicating that the diet-altered microbiota promoted colonic and hepatic MAdCAM-1 expression. $\alpha_4\beta_7$ blockade in WD-fed knockout mice significantly decreased $\alpha_4\beta_7^+$ CD4 T cell recruitment to the intestine and liver, attenuated hepatic inflammation and fibrosis, and improved metabolic indices. MAdCAM-1 blockade also reduced hepatic inflammation and fibrosis in WD-fed knockout mice. Hepatic MAdCAM-1 expression was elevated in NASH patients and correlated with higher expression of α_4 and β_7 integrins.

Conclusions: These findings establish $\alpha_4\beta_7$/MAdCAM-1 as a critical axis regulating NASH development through colonic and hepatic CD4 T cell recruitment.

Lay Summary: Nonalcoholic steatohepatitis (NASH) is an advanced and progressive form of nonalcoholic fatty liver disease (NAFLD), and despite its growing incidence no therapies currently exist to halt NAFLD progression. Here, we show that blocking integrin receptor $\alpha_4\beta_7$-mediated recruitment of CD4 T cells to the intestine and liver not only attenuates hepatic inflammation and fibrosis, but also improves metabolic derangements associated with NASH. These findings provide evidence for potential therapeutic application of $\alpha_4\beta_7$ antibody in the treatment of human NASH.

Graphical Abstract

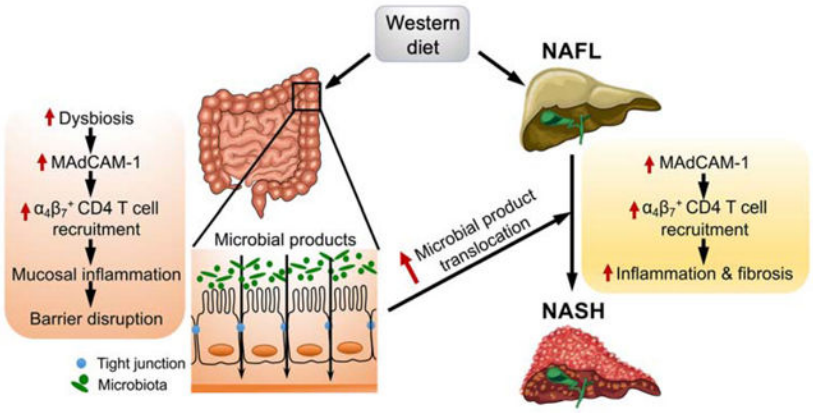

Keywords

non-alcoholic fatty liver disease; microbiota; gut permeability; epithelial barrier; inflammation

INTRODUCTION

Nonalcoholic steatohepatitis (NASH) is an advanced and progressive form of nonalcoholic fatty liver disease (NAFLD), afflicting 50 million people worldwide and over 16 million people in North America [1]. An estimated one in six patients with NASH progress to cirrhosis and recent evidence links NASH to a higher incidence of hepatocellular carcinoma [2]. While a Western diet (WD) is likely a major risk factor for NASH development, the progressive nature of the disease suggests that other ongoing biological insults or “second hits” play a significant and complex role in NASH etiology. Increased intestinal permeability has been reported in human NAFLD [3–5], and we have demonstrated that humans with NAFLD and no known inflammatory bowel disease have mucosal inflammation and decreased expression of the gene *F11r* encoding the intestinal tight junction (TJ) protein junctional adhesion molecule A in the colonic mucosa [6]. In the *F11r* knockout mouse model, feeding studies revealed development of severe NASH with significant fibrosis within eight weeks of initiating a WD. WD consumption further potentiated intestinal epithelial permeability in $F11r^{-/-}$ mice secondary to mucosal inflammation triggered by gut dysbiosis [6]. Loss of the intestinal epithelial barrier in WD-fed $F11r^{-/-}$ mice resulted in the translocation of gut bacterial products which facilitated rapid progression of NAFLD by driving hepatic inflammation and fibrosis [6]. Depletion of gut microbiota using a broad-spectrum antibiotic cocktail not only attenuated diet-induced hepatic inflammation and fibrosis but also improved metabolic derangements demonstrating a key role for gut microbiota in NASH development [6]. These data and other published work in animal models as well as human studies underscore the importance of intestinal epithelial permeability in NASH development and implicate diet-induced mucosal inflammation as a major contributor to disease progression [3–6]. However, the mechanisms underlying immune mediated mucosal inflammation in NASH have not yet been clearly defined.

The recruitment of immune cells to tissues is a highly regulated process that is essential for immune homeostasis and the resolution of inflammation following injury or infection.

Immune cell recruitment is orchestrated by adhesion molecules expressed on homing lymphocytes and their corresponding ligands expressed by endothelial cells [7]. The heterodimeric integrin receptor $\alpha_4\beta_7$ regulates intestinal T cell recruitment via interaction with its ligand MAdCAM-1 constitutively expressed by high endothelial venules and the intestinal lamina propria [7]. This process is essential for maintaining intestinal epithelial barrier function, as dysregulated CD4 T cell recruitment to the intestine can underlie mucosal inflammation leading to loss of intestinal barrier function [7–9]. While the $\alpha_4\beta_7$/MAdCAM-1 axis is implicated in promoting hepatic inflammation in other chronic liver diseases [10, 11], the contribution of this axis in mucosal and hepatic inflammation in NASH is not known.

In this study, using our recently characterized mouse model of NASH, WD-fed *F11r*$^{-/-}$ mice [6], we provide evidence for the first time that $\alpha_4\beta_7$-mediated homing of CD4 T cells to the intestine and liver promote NASH development. We demonstrate that WD promotes a systemic increase in $\alpha_4\beta_7^+$ CD4 T cells. These cells are recruited to the intestine and liver by a microbiota-driven increase in colonic and hepatic MAdCAM-1 expression. We show that blocking $\alpha_4\beta_7^+$ CD4 T cell recruitment to the intestine and liver attenuates hepatic inflammation and fibrosis and improves indices of the metabolic syndrome (MetS). Analysis of liver tissue from NASH patients revealed higher expression of *MAdCAM-1* which correlated with elevated expression of integrins α_4, *ITGA4* and β_7, *ITGB7*. Together, our results indicate that blockade of $\alpha_4\beta_7$ or MAdCAM-1 may represent a novel therapy for treating NASH patients.

METHODS

Mice.

Junctional adhesion molecule A (JAM-A) knock out mice (*F11r*$^{-/-}$) were generated as previously described [6]. Mice were bred and maintained at Emory University and the University of Pittsburgh Division of Animal Resources. All animal studies were approved by Institutional Animal Care and Use Committee.

Human tissue.

Human liver tissues were obtained from Sekisui-XenoTech, LLC (Kansas City, KS) and Biospecimen Processing and Repository Core at Pittsburgh Liver Research Centre. This study was institutional review board exempt as the human tissues used in this study were de-identified, fixed human tissue.

NASH diet:

The western diet (WD) consisted of 0.2% cholesterol, 20% protein, 43% CHO, 23% fat (6.6% trans-fat), and 2.31% fructose (TD.130885; Harlan Laboratories) [6]. The normal diet (ND) is the standard mouse chow that contains 16% protein, 61% carbohydrate and 7.2% fat. Five to six-week-old male mice were fed the WD *ad libitum* for eight-weeks to induce NASH. Littermate *F11r*$^{+/+}$ mice served as controls for all experiments.

Statistical analysis.

Statistical differences between multiple groups were analyzed by ANOVA and post hoc analysis for multiple group comparison. For $\alpha_4\beta_7$ and MAdCAM-1 blocking experiments, statistical differences between groups were analyzed by Fisher's exact test (two-sided) with post hoc analysis for pairwise comparison. A p value < 0.05 was considered statistically significant. Data shown are representative of three independent experiments. All statistics were performed using GraphPad Prism 8.0 (GraphPad Software) or R software.

RESULTS

WD consumption increases "gut tropic" CD4 T cells in the peripheral blood.

As previously reported [6], WD-fed *F11r*$^{-/-}$ mice developed NASH compared to findings of only mild steatosis in control *F11r*$^{+/+}$ mice (Supp. Fig. 1). Increased CD4 T cells in blood can reflect heightened CD4 T cell homing to inflamed tissues [12], and increased proinflammatory CD4 T cells have been reported in the peripheral blood and liver of NASH patients [13–16]. We therefore first determined if higher numbers of CD4 T cells were present in the peripheral blood of WD-fed mice. Flow cytometric analysis of the peripheral blood mononuclear cells (PBMC) from control *F11r*$^{+/+}$ and *F11r*$^{-/-}$ mice following eight-weeks of ND or WD-feeding revealed a significant increase in total CD4 T cells in the absence of changes to relative CD4 T cell frequencies in the WD fed *F11r*$^{-/-}$ mice (Fig. 1A–B; Supp. Fig. 2A). Since the integrin receptor $\alpha_4\beta_7$ directs CD4 T cell trafficking to the gut [7], we next examined peripheral blood CD4 T cells for expression of integrin receptor $\alpha_4\beta_7$. As shown in Fig. 1C and Supp. Fig. 2B, a significantly higher percentage and total number of CD4 T cells in WD-fed mice were positive for the expression of $\alpha_4\beta_7$. The frequency and the total number of $\alpha_4\beta_7^+$ CD4 T cells were higher in the WD-fed *F11r*$^{-/-}$ mice, compared to controls, but the difference in frequency did not reach statistical significance. Similarly, increased frequency of $\alpha_4\beta_7^+$ CD4 T cells, in the absence of changes in relative CD4 T cell numbers, was observed in the spleen of WD fed controls and *F11r*$^{-/-}$ mice (Supp. Fig. 3A–D). Together, these findings suggest that WD consumption results in a systemic increase in gut-tropic $\alpha_4\beta_7^+$ CD4 T cells implicating a role of $\alpha_4\beta_7^+$ CD4 T cells in NAFLD.

WD consumption increases intestinal recruitment of $\alpha_4\beta_7^+$ CD4 T cells.

Having established that $\alpha_4\beta_7^+$ CD4 T cells are increased in the peripheral blood, we next determined whether WD consumption similarly increased intestinal $\alpha_4\beta_7^+$ CD4 T cells. No differences in the total number and the frequency of CD4 T cells in Peyer's Patches (PP) were observed between ND-fed control and *F11r*$^{-/-}$ mice (Fig. 2A). However, WD feeding significantly increased the frequency and total number of CD4 T cells in PP of both control and *F11r*$^{-/-}$ mice with significantly higher numbers of CD4 T cells in *F11r*$^{-/-}$ mice (Fig. 2A). In agreement with the PBMC data, WD increased the total number and percentage of $\alpha_4\beta_7^+$ CD4 T cells in the PP of both control and *F11r*$^{-/-}$ mice, but the total number of $\alpha_4\beta_7^+$ CD4 T cells were significantly higher in the *F11r*$^{-/-}$ mice as compared to control mice (Fig. 2B). WD feeding significantly increased the frequency and total number of CD4 T cells in the colonic lamina propria (CLP) of control and *F11r*$^{-/-}$ mice with significantly higher numbers of CD4 T cells in *F11r*$^{-/-}$ mice (Fig. 2C). A significantly higher frequency and the

total number of CD4 T cells in the CLP of WD-fed *F11r*$^{-/-}$ mice relative to control mice are $\alpha_4\beta_7^+$ (Fig. 2D). WD feeding also increased the total number, but not the frequency of $\alpha_4\beta_7^+$ CD4 T cells in the CLP of control mice relative to ND fed mice (Fig. 2D). Increase infiltration of $\alpha_4\beta_7^+$ CD4 T cells in the colonic mucosa was further confirmed by laser confocal imaging demonstrating higher numbers of $\alpha_4\beta_7$ and CD4 double positive cells in the colonic mucosa of WD-fed *F11r*$^{-/-}$ mice relative to controls (Fig. 2E). Together these data imply that WD promotes recruitment of $\alpha_4\beta_7^+$ CD4 T cells to the intestine.

WD consumption increases microbiota-dependent colonic MAdCAM-1 expression.

While WD feeding resulted in a systemic increase in $\alpha_4\beta_7^+$ CD4 T cells in the control and *F11r*$^{-/-}$ mice, recruitment of these cells was higher in the colonic mucosa of WD-fed *F11r*$^{-/-}$ mice. Since endothelial MAdCAM-1 expression drives $\alpha_4\beta_7$ mediated homing of T cells to the colonic mucosa [7], we examined colonic MAdCAM-1 expression in controls and *F11r*$^{-/-}$ mice fed the WD. No difference in colonic MAdCAM-1 expression was detected between ND-fed controls and *F11r*$^{-/-}$ mice (Supp. Fig. 4A). In contrast, WD feeding increased colonic MAdCAM-1 expression in control and *F11r*$^{-/-}$ mice, but expression was markedly higher in the *F11r*$^{-/-}$ mice (Fig. 3A, C). Higher colonic MAdCAM-1 expression in the WD-fed *F11r*$^{-/-}$ mice correlated with increased infiltration of $\alpha_4\beta_7^+$ CD4 T cells (Fig. 2) suggesting that $\alpha_4\beta_7$/MAdCAM-1 dependent intestinal recruitment of CD4 T cells may promote mucosal inflammation and subsequent loss of barrier function in WD-fed *F11/r*$^{-/-}$ mice [6]. Since antibiotic treatment attenuates hepatic inflammation and fibrosis secondary to a marked reduction in colonic inflammation in WD-fed *F11r*$^{-/-}$ mice [6], we examined *MAdCAM-1* expression in the colonic tissue from antibiotic treated WD-fed *F11r*$^{-/-}$ mice. Antibiotic treatment markedly reduced colonic MAdCAM-1 expression suggesting a role of microbiota in regulating colonic MAdCAM-1 expression in NASH (Fig. 3B–C).

To determine whether changes in the microbiota composition were associated with increased colonic MAdCAM-1 expression, the cecal mucosa-associated microbiota were analyzed using 16S rRNA sequencing followed by phylogenetic analyses and a comparison of the microbial community structure using the unweighted UniFrac algorithm as described previously [6]. We analyzed mucosa-associated microbiota as they have a greater influence on mucosal homeostasis than the luminal microbiota due to mucosal proximity [17]. The mucosa-associated microbial compositions of both control and *F11r*$^{-/-}$ mice fed the ND were similar with higher abundance of *Proteobacteria*, followed by *Bacteroidetes*, *Firmicutes*, *Tenericutes* and *Deferribacteres* (Fig. 3D–E). WD consumption significantly increased *Proteobacteria* but decreased *Bacteroidetes* in the cecal mucosa of *F11r*$^{-/-}$ mice, compared to WD-fed controls and the ND-fed mice. In contrast, WD consumption did not alter the abundance of *Bacteroidetes* and *Proteobacteria* in the controls. In both controls and *F11r*$^{-/-}$ mice, WD consumption decreased *Tenericutes*. Since expansion of proteobacteria is most commonly associated with gut dysbiosis in intestinal inflammatory GI disorders [18, 19], our data suggest a link between *Proteobacteria* abundance in the colonic mucosa of WD-fed *F11r*$^{-/-}$ mice and increased colonic MAdCAM-1 expression.

Hepatic MAdCAM-1 expression is higher in WD-fed mice.

To evaluate the involvement of $\alpha_4\beta_7^+$/MAdCAM-1 mediated recruitment of CD4 T cells to the NASH liver, we assessed hepatic MAdCAM-1 expression by laser confocal microscopy (Fig. 4A–B). In agreement with a previous study showing increased MAdCAM-1 expression in the liver of mice fed a WD for 24 weeks [20], confocal images of liver tissue sections stained with MAdCAM-1 revealed marked increase in hepatic MAdCAM-1 expression in the WD-fed *F11r*$^{-/-}$ mice relative to controls (Fig. 4A–B). No difference in hepatic MAdCAM-1 expression was detected in ND-fed controls and *F11r*$^{-/-}$ mice (Supp. Fig. 4B). Treatment with broad-spectrum antibiotics, which attenuates WD-induced hepatic inflammation and fibrosis in *F11r*$^{-/-}$ mice [6], reduced hepatic MAdCAM-1 expression, strongly suggesting a role for microbiota in regulating diet-induced hepatic MAdCAM-1 expression (Fig. 4A–B). Further analysis revealed that hepatic MAdCAM-1 staining colocalized with alpha smooth muscle actin (αSMA), a key hepatic stellate cell (HSC) activation marker [21], suggesting that activated HSCs may be the primary cells expressing hepatic MAdCAM-1 in the WD-fed mice (Fig. 4C). Together, these data suggest that WD consumption induces microbiota-dependent hepatic MAdCAM-1 expression.

Intrahepatic $\alpha_4\beta_7^+$ CD4 T cells are higher in WD-fed mice.

Knowing that hepatic MAdCAM-1 expression was elevated in *F11r*$^{-/-}$ mice fed the WD, we next investigated whether there was a corresponding increase in hepatic $\alpha_4\beta_7^+$ CD4 T cell recruitment. As shown in Fig. 4D, WD feeding significantly increased the frequency and the total number of intrahepatic $\alpha_4\beta_7^+$ CD4 T cells in the *F11r*$^{-/-}$ mice, compared to controls. Increased hepatic $\alpha_4\beta_7^+$ CD4 T cell recruitment correlated with a significant increase in the total number of hepatic CD4 T cells relative to controls (Fig. 4E). However, no difference in the frequency of CD4 T cells was observed between ND and WD fed mice (Fig. 4E). WD consumption also increased CD4 T cells and $\alpha_4\beta_7^+$ CD4 T cells in the control mice, compared with the ND-fed mice, however their numbers were significantly lower in control mice and correlated with lower hepatic MAdCAM-1 expression (Fig. 4A–E). Increased infiltration of $\alpha_4\beta_7^+$ CD4 T cells in the liver was further confirmed by laser confocal imaging demonstrating higher numbers of $\alpha_4\beta_7$ and CD4 double positive cells in the liver of WD-fed *F11r*$^{-/-}$ mice. The transcript levels of integrins α_4 and β_7 were significantly higher in the WD-fed *F11r*$^{-/-}$ mice compared to controls (Fig. 4G–H). Further corroborating a role of gut microbiota in regulating $\alpha_4\beta_7$/MAdCAM-1-mediated recruitment of immune cells in the NASH liver, transcript levels of integrins α_4 and β_7 were significantly reduced in the liver of antibiotic-treated WD-fed *F11r*$^{-/-}$ mice (Fig. 4G–H). Together, these data suggest that WD consumption promotes hepatic recruitment of $\alpha_4\beta_7^+$ CD4 T cells.

Integrin $\alpha_4\beta_7$ blockade decreases recruitment of $\alpha_4\beta_7^+$ CD4 T cells to the intestine of WD-fed mice.

To confirm that integrin $\alpha_4\beta_7$ is involved in the recruitment of CD4 T cells to the intestine of WD-fed mice, we treated mice with a highly specific neutralizing monoclonal antibody (mAb) against $\alpha_4\beta_7$, which is effective in blocking migration of $\alpha_4\beta_7^+$ CD4 T cells to the intestinal mucosa [22]. Mice treated with IgG isotype served as controls. $\alpha_4\beta_7$ blockade significantly decreased the total number and frequency of $\alpha_4\beta_7^+$ CD4 T cells in the PP of

WD-fed *F11r*$^{-/-}$ mice (Fig. 5A). $\alpha_4\beta_7$ mAb treatment reduced total CD4 T cell numbers in the PP without altering the frequency of CD4 T cells (Fig. 5B). $\alpha_4\beta_7$ mAb treatment also reduced the total number of $\alpha_4\beta_7^+$ CD4 T cells in the CLP of WD-fed *F11r*$^{-/-}$ mice, but did not alter the frequency of $\alpha_4\beta_7^+$ CD4 T cells (Fig. 5C–D). Decreased infiltration of $\alpha_4\beta_7^+$ CD4 T cells in the CLP of $\alpha_4\beta_7$ mAb-treated mice correlated with a significant reduction in the transcript levels of MAdCAM-1 as well as integrins α_4 and β_7 compared with IgG controls (Fig. 5E–G). These data correlated with histological analysis of the colonic tissue showing decreased immune cell infiltration in the $\alpha_4\beta_7$ mAb-treated mice, relative to IgG treated controls (Supp. Fig. 5B). Improvement in colonic inflammation in the $\alpha_4\beta_7$ mAb-treated mice correlated with a significant increase in the transcript levels of tight junction proteins occludin and zonula occludens (ZO)-1 in the colon suggesting that $\alpha_4\beta_7$ mAb treatment improved colonic epithelial barrier function (Fig. 5H–I). Together, these data demonstrate that $\alpha_4\beta_7$ mAb treatment not only reduced mucosal inflammation in WD-fed *F11r*$^{-/-}$ mice, but also improved colonic epithelial barrier function.

Integrin $\alpha_4\beta_7$ blockade decreases hepatic recruitment of $\alpha_4\beta_7^+$ CD4 T cells in WD-fed mice.

To determine whether $\alpha_4\beta_7$ blockade decreased $\alpha_4\beta_7^+$ CD4 T cell recruitment to the liver, we analyzed hepatic CD4 T cells from IgG or $\alpha_4\beta_7$ mAb treated *F11r*$^{-/-}$ mice fed the WD (Fig. 6A). As shown in Fig 6A, four weeks of $\alpha_4\beta_7$ mAb treatment significantly reduced both the percentage and total number of intrahepatic $\alpha_4\beta_7^+$ CD4 T cells in the WD-fed *F11r*$^{-/-}$ mice suggesting that $\alpha_4\beta_7$ mAb treatment effectively blocked WD-induced recruitment of $\alpha_4\beta_7^+$ CD4 T cells to the liver. $\alpha_4\beta_7$ mAb treatment also reduced the total number of hepatic CD4 T cells, but did not affect the frequency of CD4 T cells (Fig. 6B). Decreased infiltration of $\alpha_4\beta_7^+$ CD4 T cells in the liver of $\alpha_4\beta_7$ mAb treated mice correlated with a significant reduction in the transcript levels of hepatic MAdCAM-1 as well as integrins α_4 and β_7 compared with IgG controls (Fig. 6C–E). Together, these data demonstrate that integrin $\alpha_4\beta_7$ promotes recruitment of CD4 T cells to the NASH liver.

Integrin a4b7 blockade attenuates WD-induced hepatic inflammation and fibrosis.

Next, to determine whether $\alpha_4\beta_7$ blockade also ameliorated hepatic inflammation and fibrosis in WD-fed *F11r*$^{-/-}$ mice, we performed histological analysis of liver tissue sections. As shown in Fig. 6F, hepatic steatosis and inflammation, assessed by H&E staining was ameliorated within four weeks of $\alpha_4\beta_7$ mAb treatment in WD-fed *F11r*$^{-/-}$ mice. Improvement in hepatic inflammation in $\alpha_4\beta_7$ mAb treated WD-fed *F11r*$^{-/-}$ mice was confirmed by a significant reduction in serum ALT (Fig. 6G) and AST (Fig. 6H) levels, as well as significantly decreased transcript levels of proinflammatory cytokines TNFα, interleukin (IL)-6 and IL-1β in the liver (Fig. 6I–K). $\alpha_4\beta_7$ mAb treatment resulted in a marked decrease in hepatic fibrosis determined by Sirius Red staining (Fig. 6L). Expression of key molecules associated with hepatic fibrogenesis, αSMA, tissue inhibitor of metalloproteinase 1 (TIMP-1), and collagen type I [α1 and α2] were also significantly lower in $\alpha_4\beta_7$ mAb treated WD-fed *F11r*$^{-/-}$ mice relative to IgG control demonstrating a significant reduction in HSC activation and collagen deposition (Fig. 6M–P). Further confirming a role of $\alpha_4\beta_7$/MAdCAM-1 axis in promoting hepatic inflammation and fibrosis in NASH, MAdCAM-1 blockade also reduced hepatic inflammation and fibrosis in WD-fed *F11r*$^{-/-}$ mice (Supp. Fig. 6A–L).

Integrin a4b7 blockade improves metabolic syndrome.

In addition to attenuating histological features of steatohepatitis, four weeks of $\alpha_4\beta_7$ mAb treatment also significantly improved metabolic parameters including body weight (Fig. 7A), liver (Fig. 7B), and visceral fat (Fig. 7C) weight, improved glucose tolerance (Fig. 7D) and insulin sensitivity (Fig. 7E), and reduced hepatic steatosis (Fig. 7F) in the WD-fed *F11r*$^{-/-}$ mice. To gain additional insights into the $\alpha_4\beta_7$ mAb induced changes in gene expression profile in WD-fed *F11r*$^{-/-}$ mice, we performed RNA-sequencing (RNA-Seq) analysis. Based on FDR < 0.05 and absolute log2 fold change greater than 1.5 for upregulated genes and 2/3 for downregulated gene1, 86 genes were upregulated and 93 genes were down-regulated in the liver of $\alpha_4\beta_7$ mAb treated WD-fed *F11r*$^{-/-}$ mice (Fig. 7G–I). Pathway enrichment analysis of differentially expressed genes (DEGs) by Ingenuity Pathway Analysis revealed 17 pathways that were significantly enriched (p-value ≤ 0.01) in the $\alpha_4\beta_7$ mAb treated WD-fed *F11r*$^{-/-}$ mice compared with IgG controls. Genes associated with PXR/RXR activation, LPS/IL-1 mediated inhibition of RXR function, FXR/RXR activation, xenobiotic metabolism, Aryl hydrocarbon receptor signaling and glycogen degradation III were repressed, whereas EIF2 signaling and mTOR signaling were upregulated in $\alpha_4\beta_7$ mAb treated WD-fed *F11r*$^{-/-}$ mice (Fig. 6I). Collectively, these data suggest that $\alpha_4\beta_7$ mAb treatment not only reverses hepatic inflammation and fibrosis but also improves metabolic parameters associated with NASH.

NASH patients have higher MAdCAM-1 expression in the liver.

To corroborate the human relevance of our findings we analyzed liver biopsies from NASH patients to determine the expression of MAdCAM-1 by confocal microscopy and RT-PCR. Subjects were diagnosed as having NASH if they had a body mass index (BMI) ≥ 25kg/m^2, ≥ 50% hepatic steatosis, the presence of inflammatory immune cell infiltrates and fibrosis, elevated serum AST and ALT levels, NASH-CRN score >3 and fibrosis score >4 (Fig. 8A–C). We defined controls as patients with a normal BMI, and the absence of hepatic steatosis, inflammatory immune cell infiltrates and fibrosis (Fig. 8A–C). As shown in representative micrographs, hepatic MAdCAM-1 expression was higher in NASH patients relative to the controls (Fig. 8B), and correlated with significantly higher levels of *MAdCAM1* transcripts (Fig. 8C). The transcript levels of αSMA (Fig. 8D), and integrins α_4 (Fig. 8E) and β_7 (Fig. 8F) were significantly higher in the liver of NASH patients. Together, these findings document a previously unappreciated role for $\alpha_4\beta_7$/MAdCAM-1 in the recruitment of immune cells to the liver and driving hepatic inflammation and fibrosis in NASH.

DISCUSSION

Building upon our understanding of the gut-liver axis in NASH pathogenesis, the present findings support the novel observation that $\alpha_4\beta_7^+$ CD4 T cells not only contribute to the loss of intestinal epithelial barrier in the WD-fed *F11r*$^{-/-}$ mice, but also promote hepatic inflammation and fibrosis. Our results demonstrate that consumption of a WD results in a systemic increase in $\alpha_4\beta_7^+$ CD4 T cells which are actively recruited to the gut and liver by diet-induced, microbiota-dependent intestinal and hepatic MAdCAM-1 expression. Blocking $\alpha_4\beta_7$ decreased both intestinal and hepatic recruitment of $\alpha_4\beta_7^+$ CD4 T cells, substantially reducing mucosal inflammation and hepatic inflammation and fibrosis in WD-fed *F11r*$^{-/-}$

mice. Furthermore, we demonstrate that blocking MAdCAM-1 also results in similar attenuation of hepatic inflammation and fibrosis in WD-fed *F11r*$^{-/-}$ mice. These observations suggest a previously unappreciated dual role for $\alpha_4\beta_7^+$ CD4 T cells in regulating both mucosal and hepatic inflammation in NASH.

The intestinal epithelial barrier is an important defense against luminal microbes, and the gut mucosal immune system maintains the integrity of this barrier [23]. Our data demonstrate that WD dysregulates mucosal immune homeostasis by increasing $\alpha_4\beta_7^+$ CD4 T cell recruitment to the intestinal mucosa. In concert with our observations suggesting an association between diet-induced, microbiota-dependent increase in colonic MAdCAM-1 expression and increased recruitment of $\alpha_4\beta_7^+$ CD4 T cells to the intestine, a recent study showed that whole-body MAdCAM-1 knockout mice are protected from diet-induced NASH [20]. In contrast, the same study reported more severe NASH in β_7 knockout mice, which was associated with increased hepatic MAdCAM-1 expression, but a decrease in the hepatic CD4/CD8 ratio as well as the percentage of Foxp3+ T regulatory cells [20]. The study did not take into account the established defects in the gut associated lymphoid tissue development in β_7 knockout mice [24, 25], which complicate interpretation of the data. These confounding results emphasize the inherent limitations of whole-body knockout mice in functional studies as nonspecific phenotypes in whole-body knockouts are ignored. The $\alpha_4\beta_7$ mAb used in our study is highly specific and binds a conformational epitope accessible only in the heterodimer $\alpha_4\beta_7$ [26–28]. Its specificity has been tested in multiple experimental and clinical settings, and the humanized $\alpha_4\beta_7$ mAb is an established therapy for inflammatory bowel disease [27–30]. The role of integrin receptor $\alpha_4\beta_7^+$ CD4 T cells in promoting diet-induced mucosal inflammation in NASH is of particular interest as a similar mechanism has been reported in inflammatory bowel disease where $\alpha_4\beta_7$ blockade, which reduces mucosal inflammation by decreasing recruitment of CD4 T cells to the mucosa, has become an effective therapy [27, 29, 30]. It should be noted that WD also increased recruitment of $\alpha_4\beta_7^+$ CD4 T cells to the intestine of control mice, which is associated with tight junction disruption as indicated by redistribution of the tight junction protein occludin [6]. However, we did not detect increased intestinal permeability by FITC-dextran in these mice which do not develop NASH [6], suggesting that additional second hits such as gut dysbiosis, are required for disease progression.

Little is known about the potential role of adaptive immune cells as mediators of chronic hepatic inflammation and fibrosis in NASH. Recent advances in our understanding of diseases associated with MetS including NAFLD have demonstrated that the cells of the adaptive immune system have the potential to play a significant role in NASH development and disease progression. The role of T lymphocytes may be especially important, particularly CD4 T cells that produce pro-inflammatory mediators that can regulate activation of the innate immune system [31]. Our studies demonstrated a significant increase in $\alpha_4\beta_7^+$ CD4 T cells in the liver of WD-fed *F11r*$^{-/-}$ mice which was associated with more robust hepatic inflammation and fibrosis. Our studies for the first time demonstrate the mechanistic involvement of these cells in NASH as $\alpha_4\beta_7$ mAb treatment, which reduced hepatic $\alpha_4\beta_7^+$ CD4 T cell infiltration, attenuated hepatic inflammation and fibrosis indicating $\alpha_4\beta_7$ mediated recruitment of CD4 T cells to the liver in NASH. Our data demonstrating increased hepatic MAdCAM-1 expression and increased hepatic infiltration

of α4β7+ CD4 T cells of WD-fed *F11r*$^{-/-}$ mice strongly support a role for α4β7+ CD4 T cells in promoting hepatic inflammation in NASH. Increased recruitment of α4β7+ CD4 T cells to the liver is also reported in human chronic inflammatory liver diseases [10, 11]. While further large-scale human studies are needed, increased MAdCAM-1 as well as integrins α4 and β7 expression in the liver of NASH patients suggests that the α4β7/MAdCAM-1 axis may also play a role in the recruitment of immune cells to the liver in human NASH.

In summary, our findings demonstrate for the first time provide novel mechanistic insights into the $\alpha_4\beta_7$/MAdCAM-1 axis in immune-mediated intestinal epithelial barrier disruption and hepatic inflammation in NASH. Finally, our findings provide a logical framework for targeted therapy using $\alpha_4\beta_7$ blockade for the treatment of NASH.

Supplementary Material

Refer to Web version on PubMed Central for supplementary material.

Acknowledgements.

This research project was supported in part by the University of Pittsburgh Biospecimen Processing and Repository Core and Advanced Cell and Tissue imaging Centre of the Pittsburgh Liver Research Centre supported by NIH/NIDDK Digestive Disease Research Core Center grant P30DK120531; University of Pittsburgh Center for Research Computing through the resources provided; Emory University Integrated Cellular Imaging Microscopy Core of the Emory and Children's Pediatric Research Center.

Funding: Research reported in this publication was supported by National Institutes of Health under Award Numbers K01DK110264 to RR; R01DK072564 and R01DK061379 to CP; K01OD023034, R03AI138792, R21AI34368 to SSI; R01DK044234 and R01DK111678 to MJC; and R01DK62277, R01DK100287, and R01CA204586 to SPM and NIH/NIDDK Digestive Disease Research Core Center grant P30DK120531. The content is solely the responsibility of the authors and does not necessarily represent the official views of the National Institutes of Health, the US Food and Drug Administration, the US Department of Health and Human Services, or the US Government.

REFERENCES

[1]. Estes C, Razavi H, Loomba R, Younossi Z, Sanyal AJ. Modeling the epidemic of nonalcoholic fatty liver disease demonstrates an exponential increase in burden of disease. Hepatology 2018;67:123–133. [PubMed: 28802062]

[2]. Kanwal F, Kramer JR, Mapakshi S, Natarajan Y, Chayanupatkul M, Richardson PA, et al. Risk of Hepatocellular Cancer in Patients With Non-Alcoholic Fatty Liver Disease. Gastroenterology 2018;155:1828–1837 e1822. [PubMed: 30144434]

[3]. Wigg AJ, Roberts-Thomson IC, Dymock RB, McCarthy PJ, Grose RH, Cummins AG. The role of small intestinal bacterial overgrowth, intestinal permeability, endotoxaemia, and tumour necrosis factor alpha in the pathogenesis of non-alcoholic steatohepatitis. Gut 2001;48:206–211. [PubMed: 11156641]

[4]. Miele L, Valenza V, La Torre G, Montalto M, Cammarota G, Ricci R, et al. Increased intestinal permeability and tight junction alterations in nonalcoholic fatty liver disease. Hepatology 2009;49:1877–1887. [PubMed: 19291785]

[5]. Luther J, Garber JJ, Khalili H, Dave M, Bale SS, Jindal R, et al. Hepatic Injury in Nonalcoholic Steatohepatitis Contributes to Altered Intestinal Permeability. Cell Mol Gastroenterol Hepatol 2015;1:222–232. [PubMed: 26405687]

[6]. Rahman K, Desai C, Iyer SS, Thorn NE, Kumar P, Liu Y, et al. Loss of Junctional Adhesion Molecule A Promotes Severe Steatohepatitis in Mice on a Diet High in Saturated Fat, Fructose, and Cholesterol. Gastroenterology 2016;151:733–746 e712. [PubMed: 27342212]

[7]. Habtezion A, Nguyen LP, Hadeiba H, Butcher EC. Leukocyte Trafficking to the Small Intestine and Colon. Gastroenterology 2016;150:340–354. [PubMed: 26551552]

[8]. Kurmaeva E, Lord JD, Zhang S, Bao JR, Kevil CG, Grisham MB, et al. T cell-associated alpha4beta7 but not alpha4beta1 integrin is required for the induction and perpetuation of chronic colitis. Mucosal Immunol 2014;7:1354–1365. [PubMed: 24717354]

[9]. Neurath MF. Cytokines in inflammatory bowel disease. Nat Rev Immunol 2014;14:329–342. [PubMed: 24751956]

[10]. Grant AJ, Lalor PF, Hubscher SG, Briskin M, Adams DH. MAdCAM-1 expressed in chronic inflammatory liver disease supports mucosal lymphocyte adhesion to hepatic endothelium (MAdCAM-1 in chronic inflammatory liver disease). Hepatology 2001;33:1065–1072. [PubMed: 11343233]

[11]. Hillan KJ, Hagler KE, MacSween RN, Ryan AM, Renz ME, Chiu HH, et al. Expression of the mucosal vascular addressin, MAdCAM-1, in inflammatory liver disease. Liver 1999;19:509–518. [PubMed: 10661685]

[12]. Gorfu G, Rivera-Nieves J, Ley K. Role of beta7 integrins in intestinal lymphocyte homing and retention. Curr Mol Med 2009;9:836–850. [PubMed: 19860663]

[13]. Gadd VL, Skoien R, Powell EE, Fagan KJ, Winterford C, Horsfall L, et al. The portal inflammatory infiltrate and ductular reaction in human nonalcoholic fatty liver disease. Hepatology 2014;59:1393–1405. [PubMed: 24254368]

[14]. Inzaugarat ME, Ferreyra Solari NE, Billordo LA, Abecasis R, Gadano AC, Chernavsky AC. Altered phenotype and functionality of circulating immune cells characterize adult patients with nonalcoholic steatohepatitis. J Clin Immunol 2011;31:1120–1130. [PubMed: 21845516]

[15]. Rau M, Schilling AK, Meertens J, Hering I, Weiss J, Jurowich C, et al. Progression from Nonalcoholic Fatty Liver to Nonalcoholic Steatohepatitis Is Marked by a Higher Frequency of Th17 Cells in the Liver and an Increased Th17/Resting Regulatory T Cell Ratio in Peripheral Blood and in the Liver. J Immunol 2016;196:97–105. [PubMed: 26621860]

[16]. Ferreyra Solari NE, Inzaugarat ME, Baz P, De Matteo E, Lezama C, Galoppo M, et al. The role of innate cells is coupled to a Th1-polarized immune response in pediatric nonalcoholic steatohepatitis. Journal of clinical immunology 2012;32:611–621. [PubMed: 22228550]

[17]. Zoetendal EG, von Wright A, Vilpponen-Salmela T, Ben-Amor K, Akkermans AD, de Vos WM. Mucosa-associated bacteria in the human gastrointestinal tract are uniformly distributed along the colon and differ from the community recovered from feces. Appl Environ Microbiol 2002;68:3401–3407. [PubMed: 12089021]

[18]. Shin NR, Whon TW, Bae JW. Proteobacteria: microbial signature of dysbiosis in gut microbiota. Trends Biotechnol 2015;33:496–503. [PubMed: 26210164]

[19]. Litvak Y, Byndloss MX, Tsolis RM, Baumler AJ. Dysbiotic Proteobacteria expansion: a microbial signature of epithelial dysfunction. Curr Opin Microbiol 2017;39:1–6. [PubMed: 28783509]

[20]. Drescher HK, Schippers A, Clahsen T, Sahin H, Noels H, Hornef M, et al. beta7-Integrin and MAdCAM-1 play opposing roles during the development of non-alcoholic steatohepatitis. J Hepatol 2017;66:1251–1264. [PubMed: 28192190]

[21]. Friedman SL. Hepatic stellate cells: protean, multifunctional, and enigmatic cells of the liver. Physiol Rev 2008;88:125–172. [PubMed: 18195085]

[22]. Berer K, Boziki M, Krishnamoorthy G. Selective accumulation of pro-inflammatory T cells in the intestine contributes to the resistance to autoimmune demyelinating disease. PLoS One 2014;9:e87876.

[23]. Peterson LW, Artis D. Intestinal epithelial cells: regulators of barrier function and immune homeostasis. Nat Rev Immunol 2014;14:141–153. [PubMed: 24566914]

[24]. Sun H, Lagarrigue F, Gingras AR, Fan Z, Ley K, Ginsberg MH. Transmission of integrin beta7 transmembrane domain topology enables gut lymphoid tissue development. J Cell Biol 2018;217:1453–1465. [PubMed: 29535192]

[25]. Wagner N, Lohler J, Kunkel EJ, Ley K, Leung E, Krissansen G, et al. Critical role for beta7 integrins in formation of the gut-associated lymphoid tissue. Nature 1996;382:366–370. [PubMed: 8684468]

[26]. Tidswell M, Pachynski R, Wu SW, Qiu SQ, Dunham E, Cochran N, et al. Structure-function analysis of the integrin beta 7 subunit: identification of domains involved in adhesion to MAdCAM-1. J Immunol 1997;159:1497–1505. [PubMed: 9233649]

[27]. Soler D, Chapman T, Yang LL, Wyant T, Egan R, Fedyk ER. The binding specificity and selective antagonism of vedolizumab, an anti-alpha4beta7 integrin therapeutic antibody in development for inflammatory bowel diseases. J Pharmacol Exp Ther 2009;330:864–875. [PubMed: 19509315]

[28]. Lazarovits AI, Moscicki RA, Kurnick JT, Camerini D, Bhan AK, Baird LG, et al. Lymphocyte activation antigens. I. A monoclonal antibody, anti-Act I, defines a new late lymphocyte activation antigen. J Immunol 1984;133:1857–1862. [PubMed: 6088627]

[29]. Ley K, Rivera-Nieves J, Sandborn WJ, Shattil S. Integrin-based therapeutics: biological basis, clinical use and new drugs. Nat Rev Drug Discov 2016;15:173–183. [PubMed: 26822833]

[30]. Arijs I, De Hertogh G, Lemmens B, Van Lommel L, de Bruyn M, Vanhove W, et al. Effect of vedolizumab (anti-alpha4beta7-integrin) therapy on histological healing and mucosal gene expression in patients with UC. Gut 2018;67:43–52. [PubMed: 27802155]

[31]. Zhu J, Yamane H, Paul WE. Differentiation of effector CD4 T cell populations (*). Annu Rev Immunol 2010;28:445–489. [PubMed: 20192806]

Highlights

Western diet consumption increases gut homing integrin receptor $\alpha_4\beta_7^+$ CD4 T cells in the peripheral blood.

$\alpha_4\beta_7^+$ CD4 T cells are recruited to the gut and liver by diet-induced, microbiota-dependent expression of MAdCAM-1, the ligand for $\alpha_4\beta_7$.

$\alpha_4\beta_7$ blockade attenuates hepatic inflammation and fibrosis, and improves metabolic derangements associated with NASH.

Hepatic MAdCAM-1 expression is elevated in NASH patients and correlates with higher expression of integrins α_4 and β_7 in the liver.

$\alpha_4\beta_7$/MAdCAM-1 is a critical axis regulating NASH development, and blockade of $\alpha_4\beta_7$ may represent a novel therapy for treating NASH patients

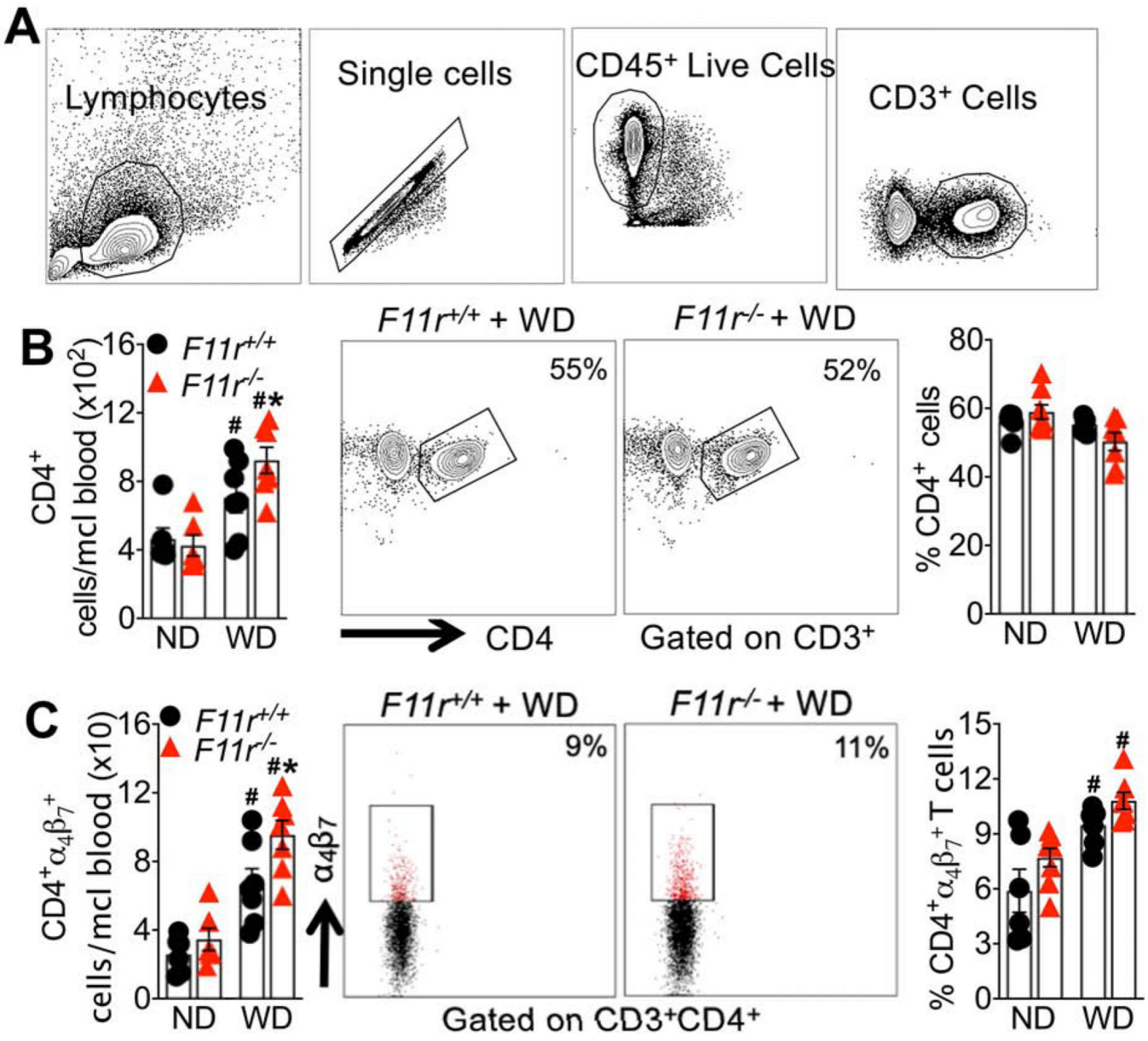

Figure 1. Western diet increases integrin $\alpha_4\beta_7^+$ CD4 T cells in the peripheral blood.

(**A**) Gating strategy for the isolation of CD4 T cells. Plots progressively gated on lymphocytes, singlets, live, CD3+, CD8+ T cells. (**B**) Representative flow plots show percent of CD4 T cells, and scatter plots show total number and percentage of CD4 T cells in peripheral blood of *F11r*$^{+/+}$ and *F11r*$^{-/-}$ mice fed a normal diet (ND) or a western diet (WD) for eight-weeks (n = 5 – 7 mice per group). (**C**) Representative flow plots show percent of $\alpha_4\beta_7^+$ CD4 T cells, and scatter plots show total number and percentage of $\alpha_4\beta_7^+$ CD4 T cells in peripheral blood (n = 5 – 7 mice per group). Data are presented as mean ± SEM. Asterisks indicate significant differences ($p < 0.05$) between *F11r*$^{+/+}$ and *F11r*$^{-/-}$ mice fed an identical diet. Hashtags indicate significant differences ($p < 0.05$) between ND or WD-fed *F11r*$^{+/+}$ and *F11r*$^{-/-}$ mice.

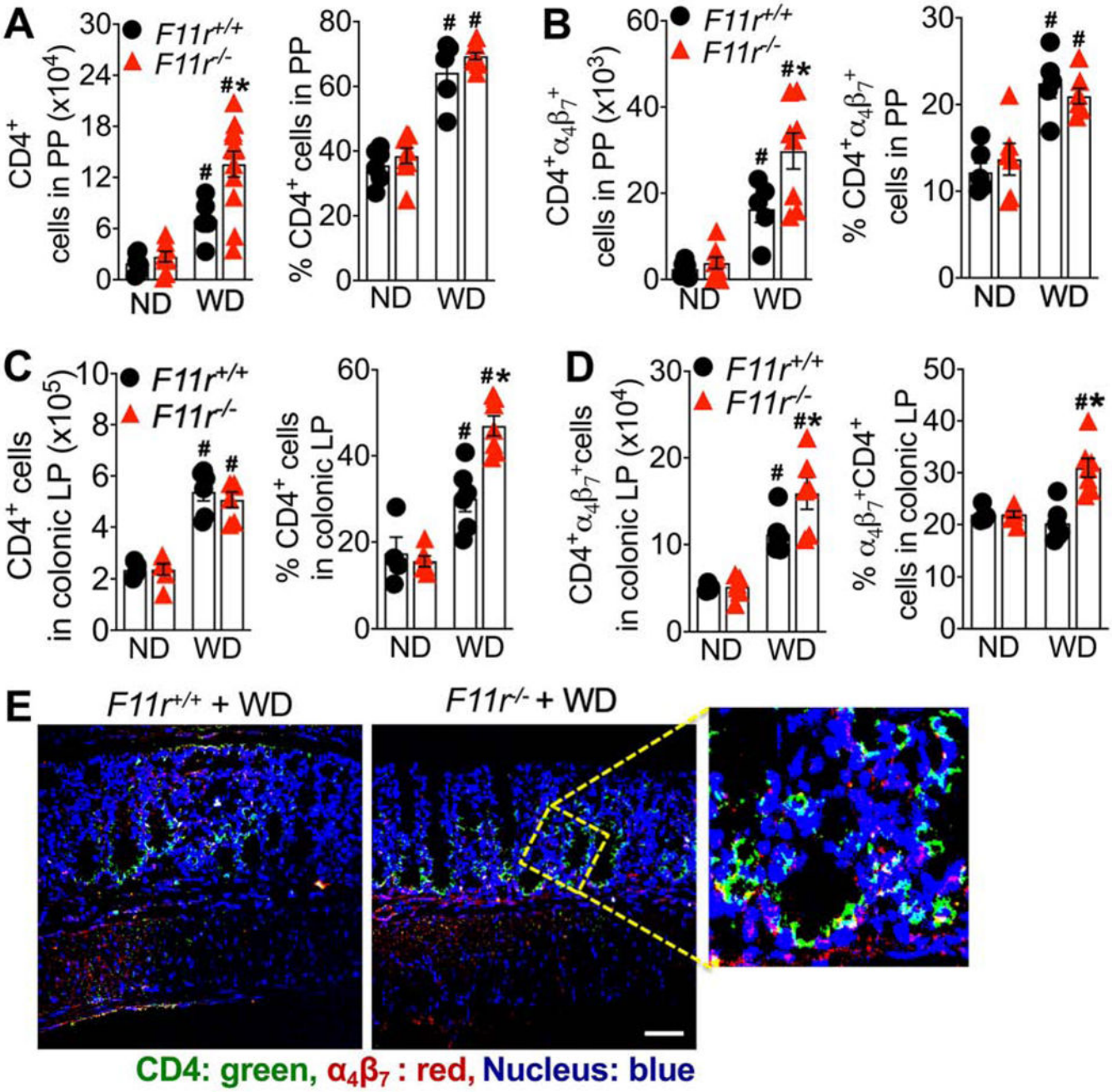

Figure 2. Western diet increases $\alpha_4\beta_7^+$ CD4 T cell recruitment to the intestine.

(**A-B**) Scatter plots show total number and percentage of (**A**) CD4 T cells (n = 5 −12 mice per group) and (**B**) $\alpha_4\beta_7^+$ CD4 T cells (n = 5 – 8 mice per group) in Peyer's patches (PP) of *F11r*$^{+/+}$ and *F11r*$^{-/-}$ mice fed a normal diet (ND) or western diet (WD) for eight-weeks. (**C-D**) Scatter plots show total number and percentage of (**C**) CD4 T cells and (**D**) $\alpha_4\beta_7^+$ CD4 T cells in the colonic lamina propria (LP; n = 4 – 6 mice per group). Data are presented as mean ± SEM. Asterisks indicate significant differences ($p < 0.05$) between *F11r*$^{+/+}$ and *F11r*$^{-/-}$ mice fed an identical diet. Hashtags indicate significant differences ($p < 0.05$) between ND or WD-fed *F11r*$^{+/+}$ and *F11r*$^{-/-}$ mice. (**E**) Representative confocal images of CD4

(green) and $\alpha_4\beta_7$ (red) immunofluorescence in the colonic mucosa of *F11r*$^{-/-}$ mice fed a WD for eight weeks (n = 5 mice per group). Nuclei are stained blue. Scale bar 100 μm.

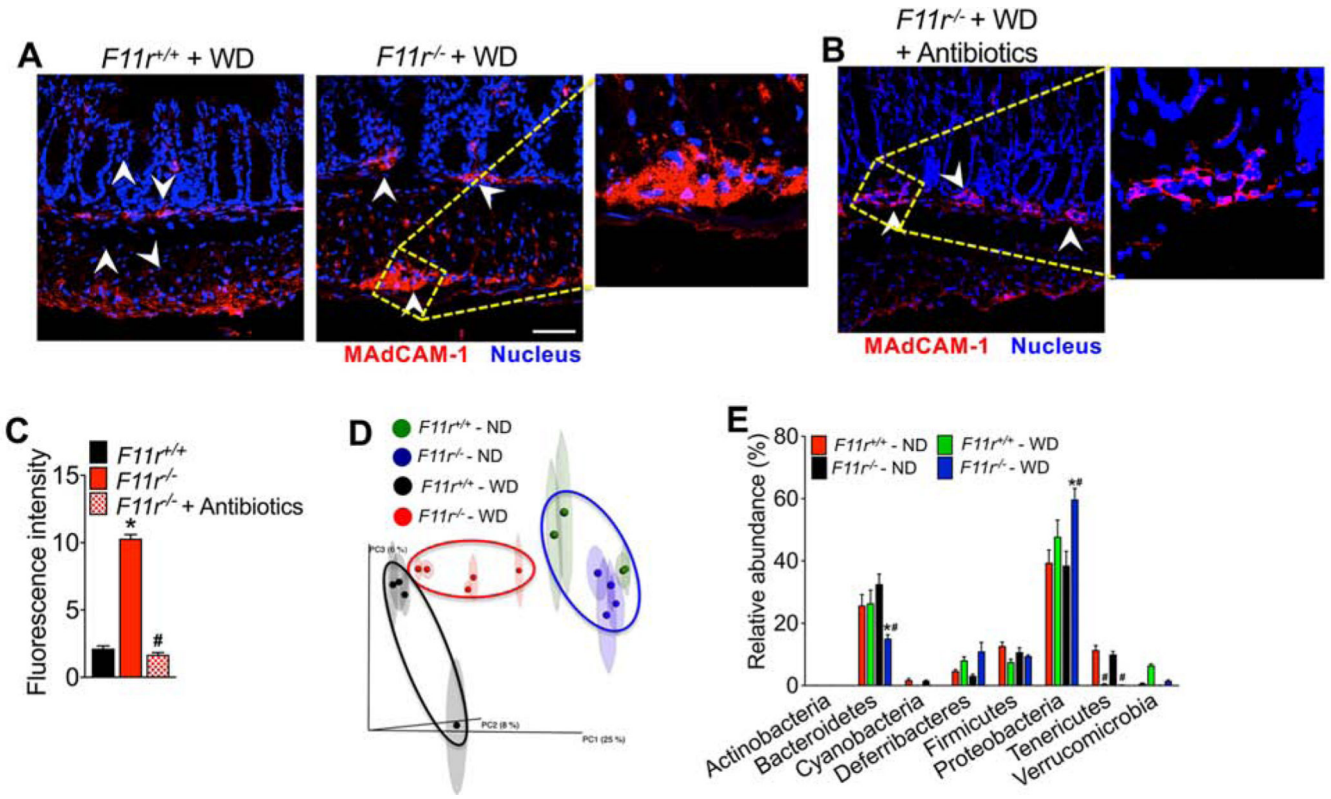

Figure 3. Western diet promotes microbiota-dependent colonic MAdCAM-1 expression.

(**A-B**) Representative confocal images of MAdCAM-1 (red) immunofluorescence in the colonic mucosa of *F11r*$^{+/+}$ and *F11r*$^{-/-}$ mice fed a western diet (WD) or WD plus antibiotics for eight-weeks (n = 5 mice per group). Nuclei are stained blue. White arrowheads, MAdCAM-1 expression. Scale bar 100 μm. (**C**) Quantification of MAdCAM-1 expression in the colon of *F11r*$^{+/+}$ and *F11r*$^{-/-}$ mice fed a WD or WD plus antibiotics for eight weeks (n = 5 mice per group). Data are presented as mean ± SEM. Asterisks indicate significant differences ($p < 0.05$) between *F11r*$^{+/+}$ and *F11r*$^{-/-}$ mice fed a WD. Hashtags indicate significant differences ($p < 0.05$) between WD or WD plus antibiotics fed *F11r*$^{-/-}$ mice. (**D-E**) Cecum mucosa-associated microbiota from *F11r*$^{+/+}$ and *F11r*$^{-/-}$ mice fed a ND or WD for eight-weeks were analyzed using 16S rRNA sequencing followed by phylogenetic analysis and a comparison of the microbial community structure using the unweighted UniFrac algorithm (n = 4 – 5 mice per group). (**D**) Jackknifed principal coordinate analysis (PCoA) of the un-weighted UniFrac distance matrix of the mucosa-associated microbiota. The ovals represent clustering by treatment groups. (**E**) Relative abundance of mucosa-associated bacterial phyla in *F11r*$^{+/+}$ and *F11r*$^{-/-}$ mice. Data are presented as mean ± SEM. Asterisks indicate significant differences ($p < 0.05$) between *F11r*$^{+/+}$ and *F11r*$^{-/-}$ mice fed an identical diet. Hashtags indicate significant differences ($p < 0.05$) between the ND or WD-fed *F11r*$^{+/+}$ and *F11r*$^{-/-}$ mice.

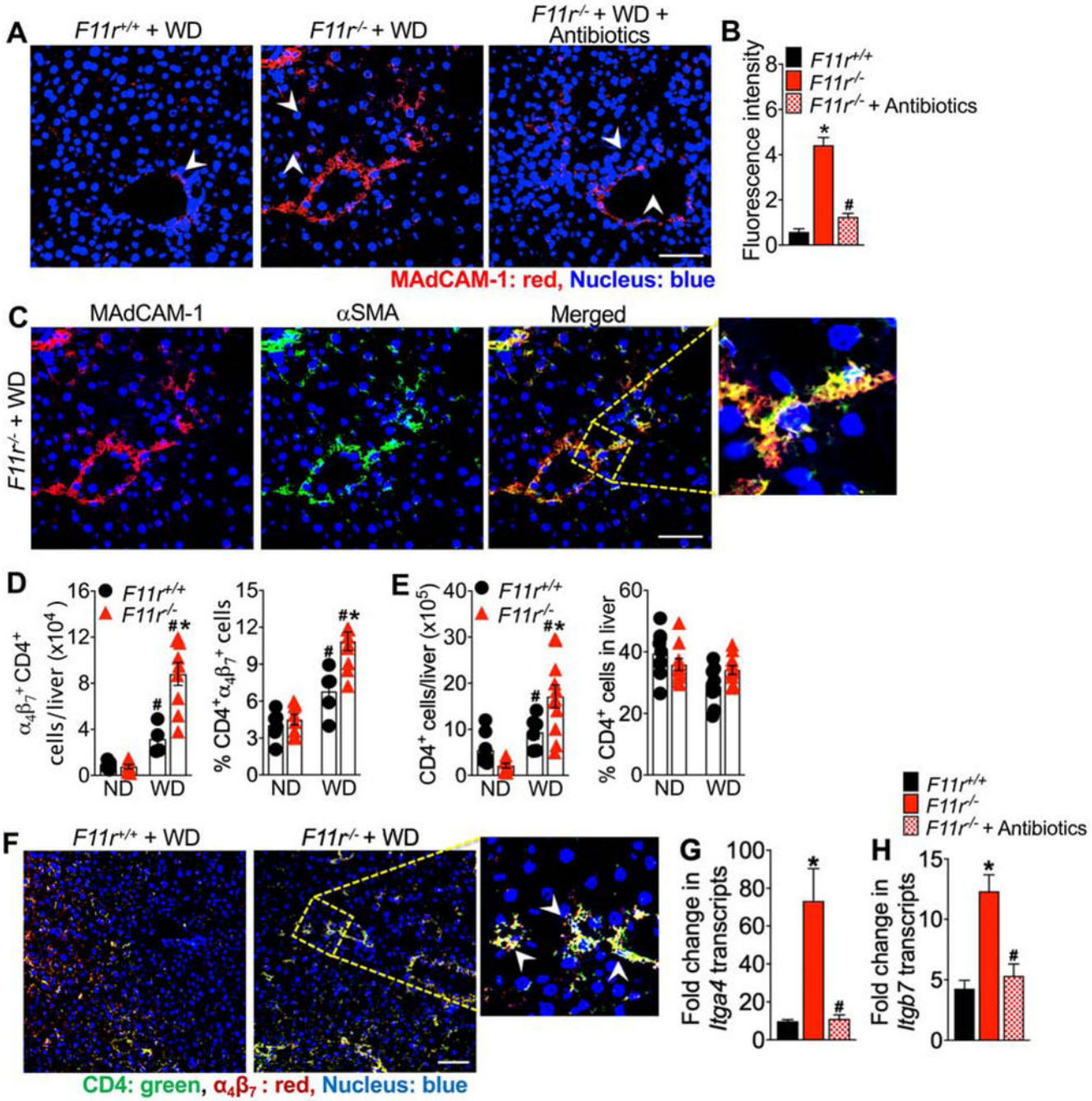

Figure 4. Western diet-induced increase in hepatic MAdCAM-1 expression is associated with increased recruitment of $\alpha_4\beta_7^+$ CD4 T cells to the liver.

(**A**) Representative confocal images of MAdCAM-1 (red) immunofluorescence in the liver of *F11r*$^{+/+}$ and *F11r*$^{-/-}$ mice fed a normal (ND) or western diet (WD), or WD plus antibiotics for eight-weeks (n = 5 mice per group). Nuclei are stained blue. White arrowheads, MAdCAM-1 expression. Scale bar 100 μm. (**B**) Quantification of MAdCAM-1 expression in the liver of *F11r*$^{+/+}$ and *F11r*$^{-/-}$ mice fed a WD or WD plus antibiotics for eight weeks (n = 5 mice per group). (**C**) Representative confocal images of MAdCAM-1

(red) and αSMA (green) immunofluorescence in the liver of *F11r*$^{-/-}$ mice fed a WD for eight weeks (n = 5 mice per group). Nuclei are stained blue. Scale bar 100 μm. (**D-E**) Scatter plots show total number and percentage of (**D**) $\alpha_4\beta_7^+$ CD4 T cells (n = 5 – 8 mice per group) and (**E**) CD4 T cells (n = 5 – 11 mice per group) in the liver of *F11r*$^{+/+}$ and *F11r*$^{-/-}$ mice fed a ND or WD for 8 weeks. (**F**) Representative confocal images of CD4 (green) and $\alpha_4\beta_7$ (red) immunofluorescence in the liver of *F11r*$^{-/-}$ mice fed a WD for eight weeks (n = 5 mice per group). Nuclei are stained blue. Scale bar 100 μm. (**G-H**) Expression of (**E**) integrin α4, *Itga4* and (**F**) integrin β7, *Itgb7* in the liver of *F11r*$^{-/-}$ mice fed a WD for eight weeks (n = 5 mice per group). Data are presented as means ± SEM. Asterisks indicate significant differences ($p < 0.05$) between *F11r*$^{+/+}$ and *F11r*$^{-/-}$ mice fed an identical diet. Hashtags indicate significant differences ($p < 0.05$) between ND or WD-fed control (*F11r*$^{+/+}$) and *F11r*$^{-/-}$ mice.

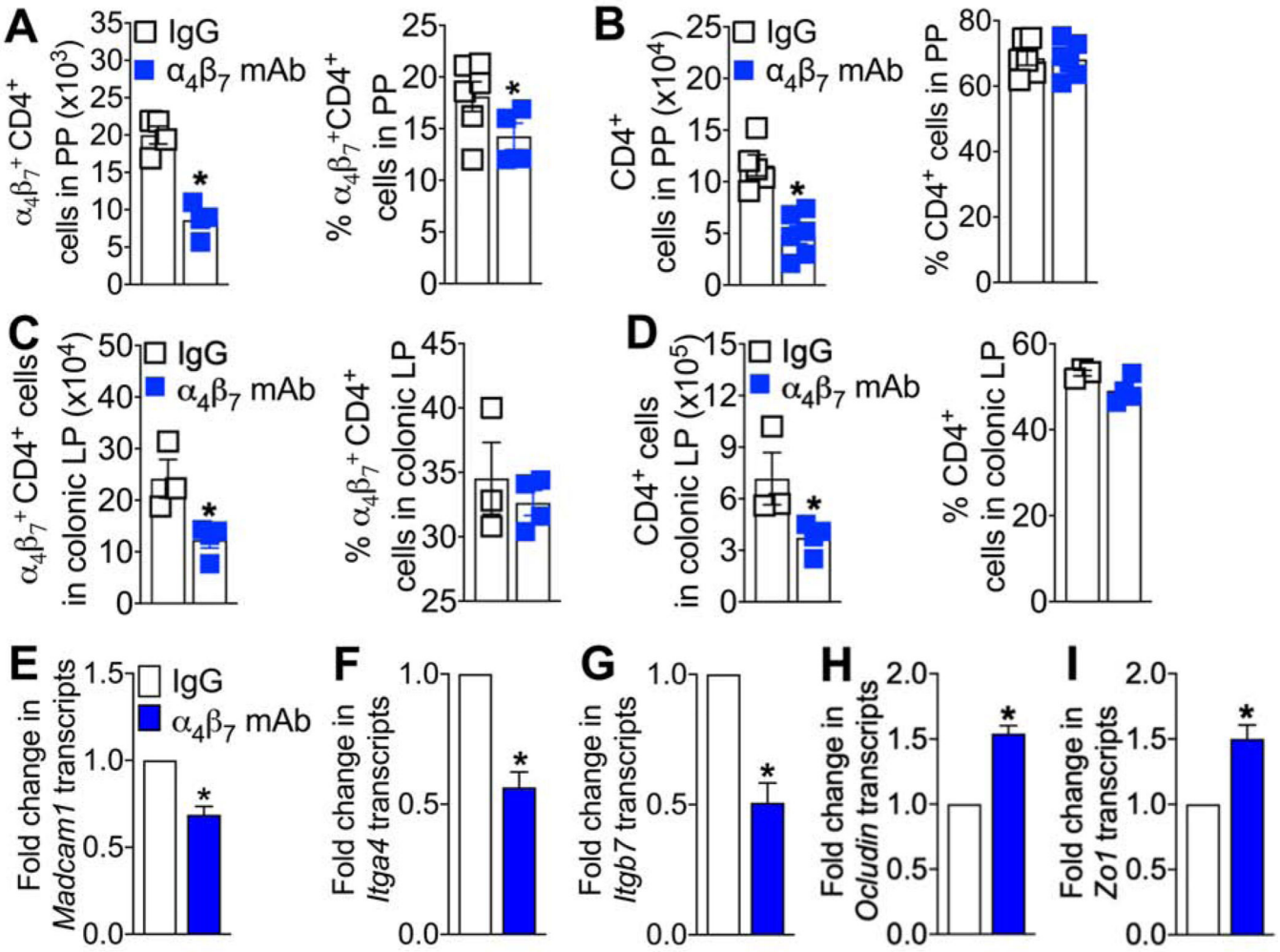

Figure 5. $\alpha_4\beta_7$ blockade decreases $\alpha_4\beta_7^+$ CD4 T cell recruitment to the intestine.

(**A-B**) Scatter plots show total number and percentage of (**A**) $\alpha_4\beta_7^+$ CD4 T cells and (**B**) CD4 T cells in the Peyer's patches (n = 4 – 6 mice per group). (**C-D**) Scatter plots show total number and percentage of (**C**) $\alpha_4\beta_7^+$ CD4 T cells and (**D**) CD4 T cells in the colonic lamina propria (LP) (n = 3 – 4 mice per group). (**E-I**) Expression of (**E**) *Madcam1*, (**F**) integrin α4, *Itga4*, (**G**) integrin β7, *Itga7*, (**H**) *occludin* and (**I**) *Zo1* in the colonic mucosa (n = 5 mice per group). *F11r*$^{-/-}$ mice fed a western diet (WD) for eight-weeks were treated with IgG or $\alpha_4\beta_7$ mAb for four weeks starting at week four after the initiation of WD. Data are presented as mean ± SEM. Asterisks indicate significant differences ($p < 0.05$) between IgG and $\alpha_4\beta_7$ mAb treatment.

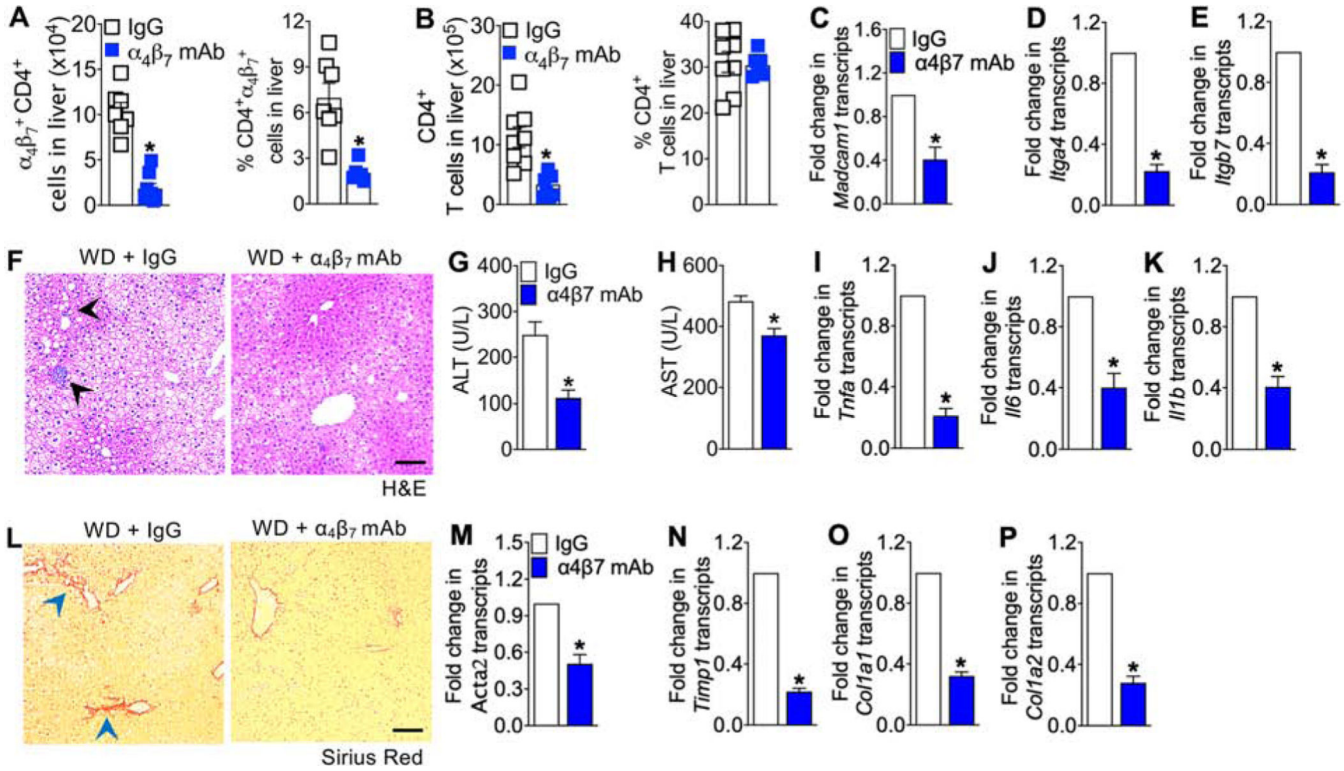

Figure 6. $\alpha_4\beta_7$ blockade attenuates hepatic inflammation and fibrosis.

(**A-B**) Scatter plots show total number and percentage of (**A**) $\alpha_4\beta_7^+$ CD4 T cells and (**B**) CD4 T cells in the liver (n = 7 – 8 mice per group). *F11r*$^{-/-}$ mice fed a WD for eight weeks were treated with IgG or $\alpha_4\beta_7$ mAb for four weeks starting at week four after initiation of the WD (n = 10 mice per group). (**C-E**) Expression of (**C**) *Madcam1*, (**D**) integrin α_4, *Itga4* and (**E**) integrin β_7, *Itgb7* in the liver (n = 5 mice per group). (**F**) Representative photomicrographs of Hematoxylin and Eosin (H&E) stained liver tissue sections. Black arrowheads, immune cells. (**G-H**) Serum ALT and AST levels. (**I-K**) Expression of key molecules associated with hepatic inflammation (n = 10 mice per group). (**L**) Representative photomicrographs of Sirius Red-stained liver tissue sections. Blue arrowheads, collagen deposition. (**M-P**) Expression of hepatic stellate cell activation markers and markers of fibrosis in the liver (n = 10 mice per group). Data are presented as mean ± SEM. Asterisks indicate significant differences ($p < 0.05$) between IgG and $\alpha_4\beta_7$ mAb treatment.

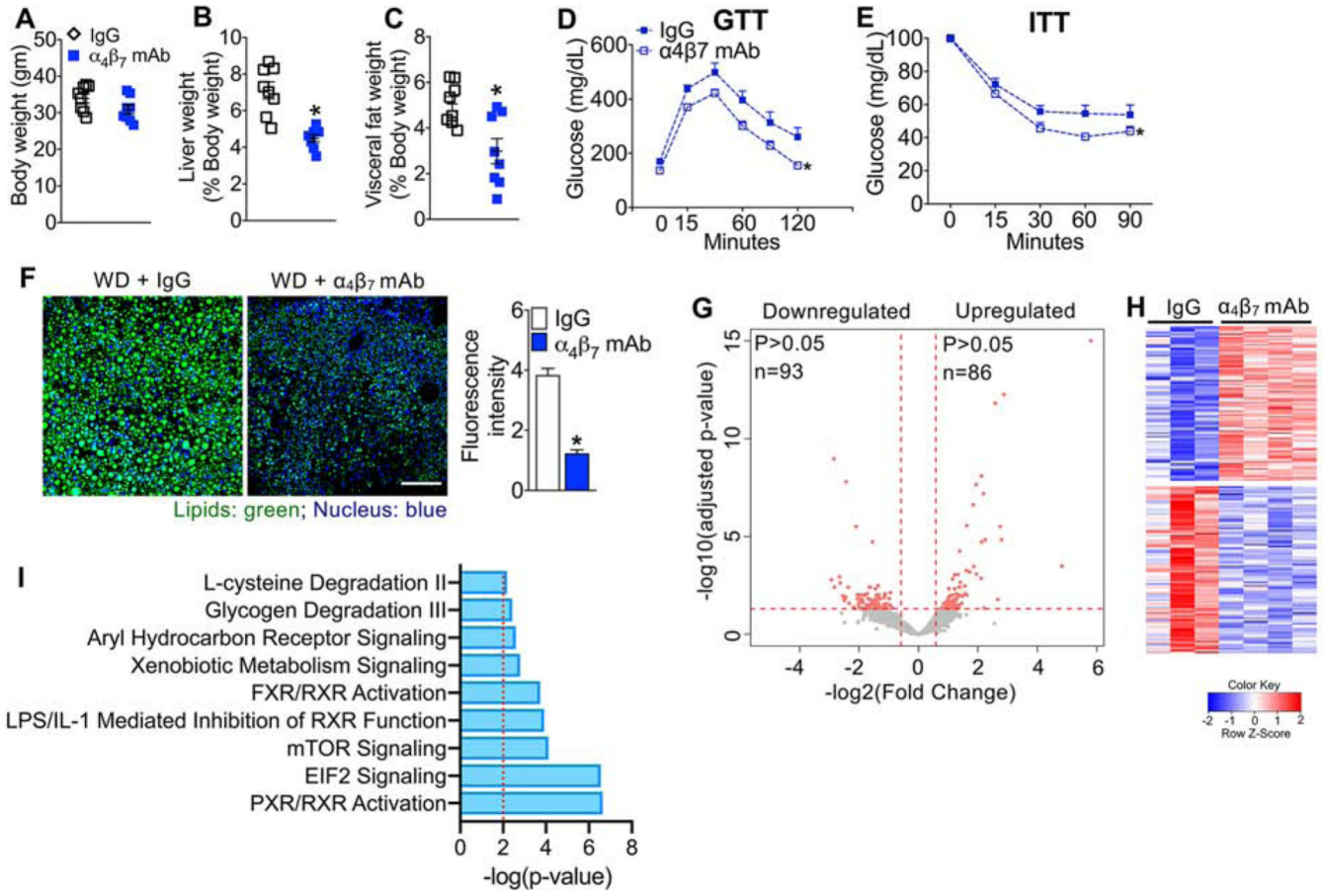

Figure 7. $\alpha_4\beta_7$ blocking improves metabolic syndrome.

Changes in (**A**) body, and (**B**) liver and (**C**) visceral fat weight reported as percent of body weight. *F11r*$^{-/-}$ mice fed a WD for eight-weeks were treated with IgG or $\alpha_4\beta_7$ mAb for four weeks starting at week four following initiation of the WD (n = 10 mice per group). (**D**) Glucose and (**E**) insulin tolerance after four weeks of IgG or $\alpha_4\beta_7$ mAb treatment (n = 5 mice per group). (**F**) Confocal microscopic images of BODIPY (lipids) stained liver tissue sections. Scale bar 20 μm. (**G**) Volcano plot showing differentially regulated genes following $\alpha_4\beta_7$ mAb treatment. (**H**) Heatmap for the differentially expressed genes. (**I**) Ingenuity Pathway Analysis of most significantly enriched signaling pathways. Data are presented as mean ± SEM. Asterisks indicate significant differences ($p < 0.05$) between IgG and $\alpha_4\beta_7$ mAb treatment.

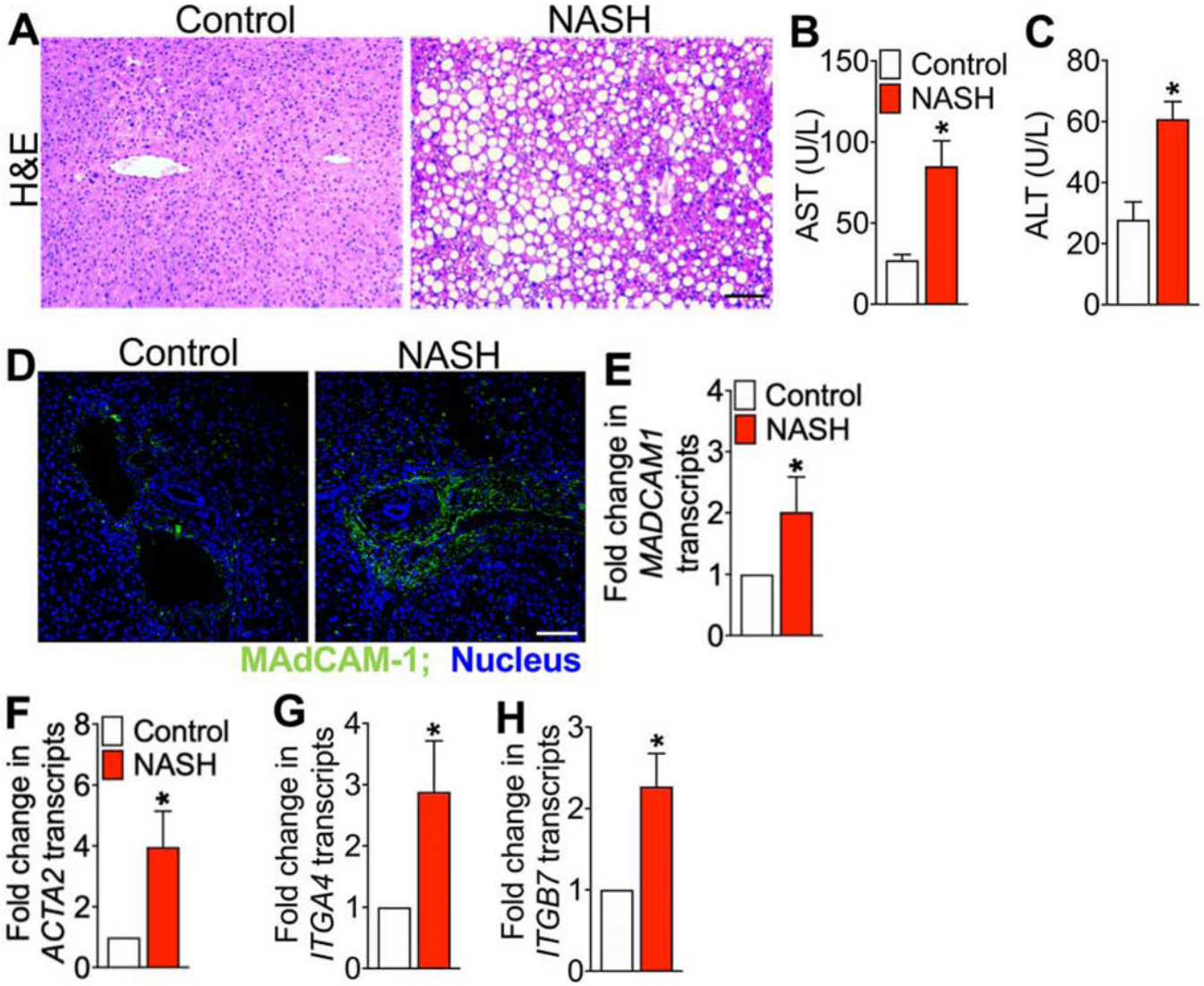

Figure 8. MAdCAM-1 expression is higher in the liver of NASH patients and correlates with increased integrin a4 and b7 expression in the liver.

(**A**) Representative photomicrographs of Hematoxylin and Eosin (H&E) stained human liver tissue biopsies obtained from NASH patients (n = 15) and subjects without NASH (controls; n = 8). Scale bar 100 μm. (**B-C**) Serum AST and ALT levels. (**D**) Representative confocal images of MAdCAM-1 (green) immunofluorescence in the liver of NASH patients and subjects without NASH. Nuclei are stained blue. Scale bar 100 μm. (**E-H**) Expression of (**E**) *MADCAM1*, (**F**) *ACTA2*, (**G**) integrin α_4, *ITGA4* and (**H**) integrin β_7, *ITGB7* in the liver (n = 5). Data are presented as mean ± SEM. Asterisks indicate significant differences ($p < 0.05$) between controls and NASH patients.